



Reagentless preparation of shape memory cellulose nanofibril aerogels decorated with Pd nanoparticles and their application in dye discoloration

Jin Gu^{a,b}, Chuanshuang Hu^a, Weiwei Zhang^a, Anthony B. Dichiara^{b,*}

^a College of Materials and Energy, South China Agricultural University, Guangzhou, Guangdong 510642, China

^b School of Environmental and Forest Sciences, University of Washington, Seattle, WA 98195, USA

ARTICLE INFO

Keywords:

Nanocellulose
Aerogel
Palladium nanoparticles
Dye discoloration

ABSTRACT

An environmentally benign method was reported for synthesizing highly porous cellulose nanofibril (CNF) aerogels decorated with palladium nanoparticles (PdNPs). Small PdNPs (< 25 nm in diameter) were successfully immobilized and reduced on the CNF surface by simply mixing the TEMPO-oxidized CNF dispersion with the palladium precursor solution and heating the aqueous mixture to 80 °C for 2 h. The resulting CNF-PdNPs hybrids could self-assemble into water-activated shape memory aerogels by freeze-drying the nanohybrid suspension. The as-prepared hybrid aerogels were successfully applied to the catalytic discoloration of aqueous cationic and anionic dye solutions in batch and dynamic column processes. The CNF-PdNP aerogels exhibited very high catalytic activity and could be conveniently separated from the products and reused with 91–99% discoloration efficiency for multiple cycles. No obvious deterioration of the material properties and structural integrity was observed during testing, hence demonstrating great potential for practical environmental remediation and catalytic applications.

1. Introduction

Nanocelluloses are a class of renewable nanomaterials prepared from the most abundant natural polymer on earth. Their outstanding mechanical properties, biorenewability, light weight, large surface to volume ratio and surface reactivity make nanocelluloses excellent nano-building blocks for ultra-light and highly porous aerogels. Nanocellulose aerogels have gained a lot of interest and have recently been reviewed [1]. They are typically derived from wet gels by supercritical or freeze drying and show promising applications in absorbents [2–5], template materials [6,7], insulation [8] and gas filtration [9] etc. The 3D adjustable network of nanocellulose aerogels can potentially serve as support for physical or chemical immobilization of different types of organic molecules [10–13] and inorganic particles [14,15] to realize the desirable functions. In particular, the latter have attracted considerable attention for their promising applications in catalysis, optics, electronics and biomedical [16]. For instance, metal nanoparticles have been employed for hydrogenation reactions [17,18], cross-coupling [19–21], discoloration of organic dyes [22], as well as sensors [23,24] and antibacterial materials [25]. However, metal nanoparticles are unstable on their own because their large active surface area leads to self-aggregation, which hinders their properties and limits practical applications. The synthesis of monodisperse metal

nanoparticles requires the use of capping agent, reducing agent, and reaction solvent, typically involving the utilization of toxic chemicals with possible deleterious effects for health and the environment [26]. A great challenge associated with the synthesis of metal nanoparticles consists of reducing the environmental footprint and eliminating the use of hazardous materials. Here we propose an environmentally benign approach to decorate highly porous nanocellulose aerogels with metal nanoparticles under mild conditions using nontoxic water as solvent. Nanocellulose can substitute both capping and reducing agents by acting as a support to immobilize and reduce metal nanoparticles, preventing their aggregation without blocking access to the reactive surface atoms [27].

Nanocellulose supports for catalytic applications are appealing due to their high surface area, stability in solvents, biodegradability, non-toxic nature and chiral properties that may participate in catalytic selection [16]. Recently, nanocelluloses have been reported as both reducing agents and stabilizers for the synthesis of palladium [21,22], silver [15,28–31], gold [32], platinum [31] and other metals [33,34] nanoparticles. The surface hydroxyl and/or sulfate ester groups play a key role in the reduction of metal species [16]. However, a relatively long processing time and/or high pressure and temperature are usually involved if nanocellulose is employed as the sole reducing agent [16,21,32]. External reducing agents, such as highly reactive N₂H₄,

* Corresponding author.

E-mail address: abdichia@uw.edu (A.B. Dichiara).

KBH_4 or H_2 , are often introduced to catalyze the reaction, which could have harmful effects for health and the environment [16,18,20]. Furthermore, previous studies have primarily focused on functionalizing nanocellulose in a solvent dispersion with metal nanoparticles or metal nanoclusters. Conforming nanocellulose into three-dimensional (3D) structures with high specific surface area could improve their immobilization and reduction properties and allow the metal nanoparticles to be easily recovered after their utilization in catalytic reactions. These 3D hybrid nanomaterials would also exhibit superior catalytic performance due to the improved diffusion of reactants through the polymeric matrix [15]. In addition, the size and morphology of the metal nanoparticles can be controlled by varying the amount of reactants, crosslinker, and functionality of the cellulose networks. Despite the above listed advantages, only few studies have reported the functionalization of nanocellulose aerogels with silver nanoparticles [15,29]. Developing a green and one-pot synthesis method to prepare an efficient and recyclable catalyst from renewable and abundant cellulose is environmentally and economically compelling.

In this research, we examine the immobilization and reduction of palladium nanoparticles (PdNPs) on TEMPO-oxidized cellulose nanofibril (CNF) aerogels based on a simple and environmentally benign method. Although the present study focuses on PdNPs, the results may be easily extended to other types of metal particles. The high binding capability and the reduction mechanism of CNF toward Pd (II) were investigated and discussed. The as-prepared water activated shape memory cellulose nanofibrils aerogels decorated with PdNPs were thoroughly characterized by electron microscopy (SEM, TEM), atomic force microscope (AFM), X-ray diffraction (XRD), UV-vis absorption spectroscopy and energy dispersive spectroscopy (EDS). To exemplify their superior catalytic properties, the CNF-PdNP aerogels were applied for the degradation of both anionic (*i.e.* Congo red, CR) and cationic (*i.e.* methylene blue, MB) dyes under mild conditions for multiple regeneration/desorption cycles.

2. Experimental

2.1. Materials

Bleached softwood pulp (WestRock Company) was obtained from a mixture of hemlock and Douglas fir. Hydrochloric acid (HCl, 0.1 N, certified, Fisher Chemical), palladium chloride (PdCl_2 , 99.9%, Alfa Aesar), sodium hydroxide (NaOH , 1 N, certified, Fisher Chemical), sodium hypochlorite (NaClO , 12.5%, BDH, VWR Chemical), 2,2,6,6-tetramethylpyperidine-1-oxyl (TEMPO, Merck), sodium bromide (NaBr , 99%, ACS, Strem Chemicals), acetic acid (Glacial, AR, Macron Fine Chemicals), sodium chlorite(NaClO_2 , 80%, Alfa Aesar), sodium borohydride (NaBH_4 , ACS, BDH, VWR Chemical), methylene blue (Tokyo Chemical Industry Co.), Congo red (MP Biomedicals LLC) were used as received. Water used was purified by Milli-Q plus water purification system (Millipore Corporate).

2.2. Preparation of cellulose nanofibrils

Softwood pulp of 30 g was soaked in 2 L DI water overnight and then disintegrated at 30,000 rpm for 10 min. Cellulose nanofibrils (CNFs) were prepared by TEMPO mediated oxidation followed by mechanical defibrillation of the pulp. Briefly, slurry containing 1 g of dry pulp, 0.016 g of TEMPO and 0.1 g of NaBr were mixed in an aqueous system of 100 mL. Oxidation reaction was initiated by adding 5 mM NaClO and conducted at 9.8–10.2 pH adjusted by adding 0.5 M NaOH . The reaction lasted until no further decrease in pH. The TEMPO-oxidized cellulose dispersion was pH adjusted to 7 with 0.1 M HCl, centrifuged at 5000 rpm for 15 min (Allegra 25R Centrifuge, Beckman Coulter), and dialyzed against water for five days. The suspension of 0.2 wt% was mechanically blended using a household blender (Osterizer,

Sunbeam Products, Inc.) set at liquefy mode for 30 min and then sonicated for 2 min using a probe sonicator (750 W, 100% amplitude, Sonics Vibracell VCX) equipped with a 13 mm stepped tip. After that, the suspension was centrifuged at 5000 rpm for 15 min to obtain supernatant.

2.3. Preparation of CNF-PdNP hybrids and CNF-PdNP aerogels

PdCl_2 solid was dissolved in 20 mM HCl at 60 °C for 1 h. The PdCl_2 concentrations were prepared to be 0.2 mM, 2 mM or 20 mM. PdCl_2 solutions of 50 mL were added dropwisely to CNF suspensions (0.2 wt %) of 50 mL under vigorous stirring and the mixture was heated to 80 °C for 120 min. The Pd concentrations in the mixtures were 0.1 mM, 1 mM or 10 mM and the CNF concentration was 0.1 wt%. The CNFs formed small gel granules at acidic condition under mechanical stirring. The excess PdCl_2 and the unbound Pd nanoparticles (PdNPs) were removed by dialysis of the mixtures against DI water for 5 days using regenerated cellulose membranes (MWCO: 12–14 KDa, Spectrum Laboratories, Inc.). Water outside the membrane was changed twice a day and the pH of the suspension was adjusted to neutral using 0.02 N NaOH on the fourth day of dialysis. After dialysis, the mixtures were placed on a magnetic stirrer operated at 1500 rpm for 6 h to break up the aggregated CNF particles, and the resulting dispersions remained stable without any precipitation for more than 5 days.

CNF-PdNP aerogels were prepared only from the mixture containing 10 mM Pd. The CNF-PdNP dispersion was concentrated to 4 mg CNF per mL and frozen at -5 °C for 24 h in a 15 mL polypropylene centrifuge tube. The CNF-PdNP aerogels were obtained by freeze-drying (FreeZone Freeze dryer, Labconco). For comparison purposes, CNF aerogels were also prepared without PdNPs by subsequently mixing, dialyzing and freeze-drying CNF suspension with 20 mM HCl under the same conditions.

2.4. Characterization

Aqueous CNF suspensions were used to measure the carboxylate and aldehyde concentrations by conductometric titration. Air-dried CNF-PdNP samples from aqueous suspensions were for PdNP morphology by transmission electron microscopy (TEM). Frozen (-5 °C) and freeze-dried (-50 °C) solids were characterized by scanning electron microscopy (SEM) and X-ray diffraction (XRD).

The carboxylate content of the CNF were measured by conductometric titration (Oakton CON 6+, Cole-Parmer Instrument Company) following a previous method [35]. The aldehyde content was determined by post NaClO_2 oxidation of TEMPO-oxidized CNF [36]. Basically, the additional carboxylate groups formed by the post NaClO_2 oxidation of CNF were regarded as the amount of aldehyde content in the original CNF.

TEM samples were prepared by depositing 10 μL drop of 0.01% aqueous suspension of CNF-PdNPs onto carbon-coated TEM grids (300-mesh copper, formvar-carbon, Ted Pella Inc.). The excess liquid was removed by blotting with a filter paper after 10 min. An FEI TECNAI G2 F20 S-TWIN high resolution transmission electron microscope operated at 100 kV accelerating voltage was used to obtain the morphology and crystal structure of the PdNPs loaded on CNF. The images were processed through Image J and the size distribution of the PdNPs was determined from more than 300 individual nanoparticles. The size was measured by the widest part of individual nanoparticles.

Surface morphology of freeze-dried CNF and CNF-PdNP aerogels was examined by a scanning electron microscope (SEM, XL830, FEI Company, Hillsboro, OR, USA) operated at 5 kV accelerating voltage and 5 mm working distance. The samples were coated with a thin layer of platinum before imaging. Elemental analysis was performed by an energy dispersive X-ray spectrometer (EDS) attached to the SEM.

The Pd content of the CNF aerogels was measured by inductively coupled plasma mass spectrometry (ICP-MS, Perkin Elmer ELAN-

DRCe). The samples were digested using nitric acid and hydrogen peroxide (3:1 v/v) with a microwave digester at 1400 w for 30 min. The resultant solutions were diluted to a ppb level of 10 for ICP-MS analysis.

XRD profile of freeze-dried CNF-PdNP was obtained with a Bruker D8 X-ray powder diffractometer using a Ni filtered Cu-K α radiation generated at 40 kV and 40 mA. The freeze-dried solid was pressed to a film before the measurement. Diffractograms were collected at a rate of 2 degrees/min from 10 to 90 degrees two theta. The Pd crystallite dimension of (111), (200), and (311) planes were calculated based on the Scherrer equation shown below,

$$B_{hkl} = \frac{K\lambda}{\cos\theta\Delta2\theta} \quad (1)$$

where B_{hkl} is the average crystalline width of a specific plane (hkl); K is a constant depending on the method of taking the breadth (K = 0.9 is used); λ is the wavelength of incident X-rays ($\lambda = 0.15406$ nm); θ is the corresponding Bragg angle; $\Delta2\theta$ (in radius) is the FWHM of the reflection peak and it is determined by peak deconvolution using OriginPro software.

UV-vis spectroscopy (Perkin Elmer Lambda 750) was used to monitor the reduction of Pd(II) by CNF and the catalytic performance of the aerogels as a function of time, by estimating the solution concentrations at the maximum absorption peaks for Pd(II), MB and CR using a measured extinction coefficient from Beer's law analysis. The optical path of the quartz cuvette was 1 cm.

2.5. Catalytic reduction of dyes

In a typical batch experiment, CNF-PdNP aerogel of ~1.0 mg was added into 3 mL of mixed solution containing 2 mL 30 mg/L dye and 1 mL 40 mg/L NaBH₄ in a quartz cuvette, which was placed in the sample holder of the UV-vis spectrophotometer during the measurement. During the measurement intervals, the cuvette was placed on an orbital shaker operated at 120 rpm to accelerate the mass transfer process. The discoloration reaction was monitored by recording the time-dependent absorbance spectra in the range of 525–725 nm for MB, and 250–600 nm for CR with a 2 nm resolution. The catalytic turnover frequency was calculated as the number of reduced dye moles (mol) per mole of Pd (mol⁻¹) per minute (min⁻¹), where the number of active catalytic sites was assumed to be the total number of Pd atoms for simplicity. For comparison purposes, experiments were also conducted in the absence of either PdNPs or NaBH₄.

To study the reusability of the CNF-PdNP aerogels, the spent CNF-PdNP aerogels were squeezed with tweezers and placed into another 3 mL of solution containing the same concentration of dye and NaBH₄. The performance of the aerogels was monitored for five repeating squeezing/discoloration cycles by UV-vis absorption spectroscopy. The maximum absorption peaks for MB at 664 nm and for CR at 498 nm were used to calculate the reaction rate and discoloration efficiency for each cycle.

For continuous flow treatment demonstration, a gravity-fed column packed with ~5.0 mg CNF-PdNP aerogel was operated with an aqueous mixture containing 6.7 mg/L MB and 33.3 mg/L NaBH₄. For packing purposes, the packed column was pre-wet with DI water and a gentle press was applied to the wet gel to ensure perfect contact between the aerogel and the delivery tip of the column. The discoloration efficiency was determined at room temperature by measuring the effluent concentration at the outlet of the column by UV-vis absorption spectroscopy.

3. Results and discussion

3.1. Reduction of Pd (II) by CNF

CNFs prepared from bleached softwood pulp were usually 1–5 nm thick and 300–600 nm long as indicated by AFM (Fig. S1). The

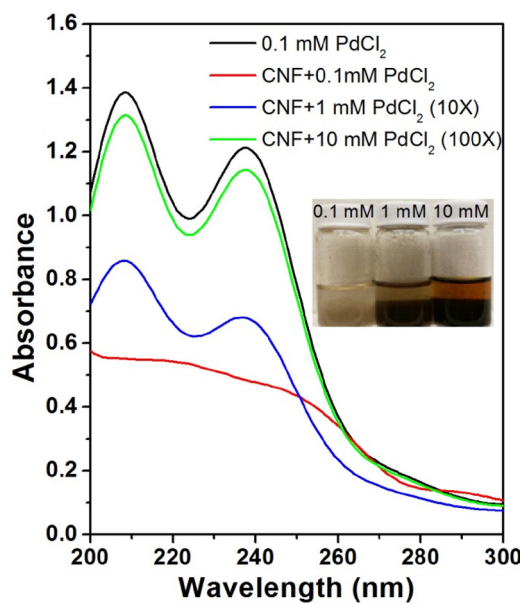


Fig. 1. UV-vis spectra of 0.1 mM PdCl₂, the supernatants of 0.1 wt% CNF after hydrothermal reacting with 0.1 mM PdCl₂, 1 mM PdCl₂ (diluted 10 times) and 10 mM PdCl₂ (diluted 100 times), respectively. The inset is a photograph of CNF and PdCl₂ mixtures after hydrothermal reaction with different Pd concentrations.

carboxylate content of the CNF was 0.98 mmol/g or 0.16 per anhydroglucose, as measured by conductivity titration (Fig. S2). The aldehyde content of the CNF was 0.28 mmol/g as determined from post NaClO₂ oxidized CNF (Fig. S2). These values are consistent with previous reports about TEMPO-oxidized CNFs [37]. The nano-sized and negatively charged CNF could help stabilize the positively charged Pd (II) by electrostatic interaction, while aldehyde groups showed reduction potential.

The reduction of Pd (II) by CNFs was observed by naked eyes and monitored by the UV-vis absorption spectroscopy (Fig. 1). PdCl₂ solution of 0.1 mM exhibited an obvious absorption peak at 234 nm, corresponding to PdCl₄²⁻. After reaction at 80 °C for 2 h and sitting at the room temperature for 3 h, CNFs in the mixture settled as gelled particles at the bottom (Fig. 1, inset). The color of the CNF precipitates turned darker with increasing PdCl₂ concentration (*i.e.* light grey for CNF reacted with 0.1 mM PdCl₂ and dark brown for CNF reacted with 10 mM PdCl₂), indicating more Pd metal was deposited on the surface of the CNFs at higher Pd precursor concentration. The supernatants of the mixtures were studied by UV-vis spectroscopy. The PdCl₄²⁻ absorption peak of the supernatant from 0.1 mM PdCl₂ and CNF mixture almost disappeared, which is consistent with the reduction of Pd(II) to Pd (0) [22]. Since the supernatant still contained a small amount of CNFs, which were able to absorb UV light [35], a broad peak around 200–270 nm could still be observed. The supernatants from 1 mM PdCl₂ and 10 mM PdCl₂ mixtures were diluted 10 times and 100 times, respectively, before the UV-vis measurements. The spectra indicate that with increasing PdCl₂ concentration, more Pd (II) remained in the supernatant. When the PdCl₂ concentration was 10 mM, the reactant was in large excess. CNF loaded with the highest amount of Pd metal at 10 mM Pd concentration was chosen for future morphology, crystal structure and catalytic analysis.

To further understand the reduction mechanism of CNF, two types of cellulose materials, including the softwood pulp before TEMPO oxidation and the NaClO₂ post oxidized CNF were also reacted with PdCl₂ solution of 1 mM, respectively, in the same conditions as that of CNFs. The UV-vis spectra of the supernatants (diluted 10 times) and digital photograph of the mixtures after hydrothermal reaction were recorded (Fig. S3). No Pd metal deposition was formed in the softwood

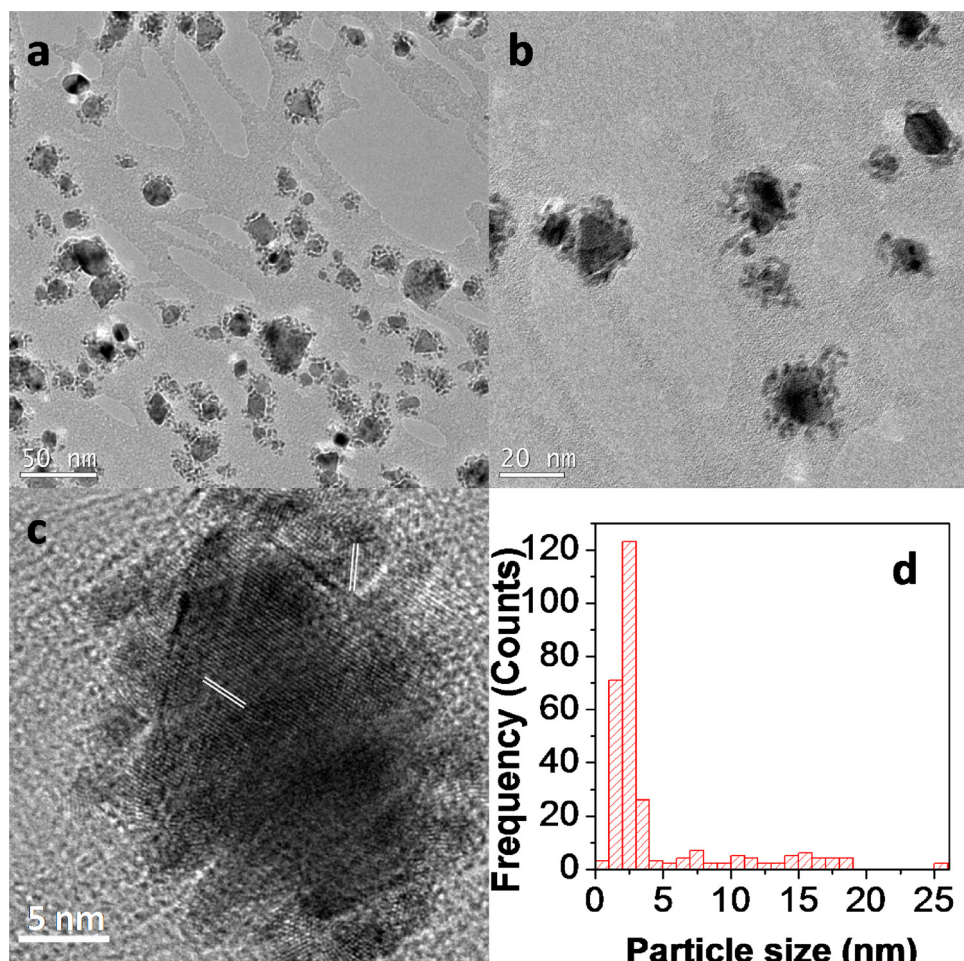


Fig. 2. Representative TEM images of PdNPs supported on CNFs (a–c) and the size distribution of PdNPs (d).

pulp mixture. NaClO₂ post oxidation was able to convert all the aldehyde groups in TEMPO-oxidized CNFs into carboxyls [36]. Compared to the original CNF, much less Pd metal was formed in the NaClO₂ oxidized CNF mixture. These results indicate that TEMPO oxidation and perhaps the following mechanical defibrillation of the pulp produced more surface reducing groups. Aldehyde content functions as an effective agent to reduce Pd(II) ions to PdNPs, while the reducing ends hemiacetal groups or hydroxyl groups in cellulose may also play minor roles.

The morphology of PdNPs was studied by transmission electron microscopy (Fig. 2). It can be seen that CNFs form bundles in the presence of PdNPs during the drying process. PdNPs with different sizes and shapes were located on the surface of CNF bundles. The Pd metal tended to form clusters comprising several individual nanoparticles with a diameter of 1–3 nm. Sometimes a large polyhedron nanoparticle with a dimension of 5–25 nm could be seen at the center of the clusters. One cluster contained at least tens of small PdNPs. The formation of PdNP clusters may be due to the high Pd precursor concentration used.

The crystalline structure of the PdNPs was studied by high resolution TEM (HRTEM). Fig. 2c shows the HRTEM images of a PdNP cluster. The space of the atomic lattice fringes is about 0.24 nm, which is consistent with Pd crystal. The large nanoparticle at the center of the cluster exhibits clear co-directionally arranged atomic lattice fringes, demonstrating a single crystalline character. However, at the edge of the cluster, the atomic lattice fringes are randomly ordered, which may correspond to the random stacking of individual small nanoparticles. Randomly ordered lattice fringes can also be seen in cluster containing only tiny PdNPs with diameter of 1–3 nm. These results are consistent

with previous work reporting the synthesis of PdNPs with various shapes of polyhedrons and spheres using different reductants and stabilizers [38,39]. Similar cluster structure of PdNPs has also been reported using cellulose nanocrystals as both reductant and support [22].

X-ray diffraction was used to further investigate the crystal structure of CNF-PdNP hybrid (Fig. 3). The diffraction peaks at 40.0°, 46.3°, 68.0°, 82.1° and 86.4° correspond to Pd (111), Pd (200), Pd (220), Pd (311) and Pd (222), respectively, again confirming the successful reduction of Pd (II) to Pd (0). Typical cellulose I characteristic peaks at 2θ = 14.8°, 16.5° and 22.5° corresponding to (110), (110), and (200) lattice planes were also observed, indicating that the deposition of PdNPs onto CNFs did not change the cellulose crystalline structure.

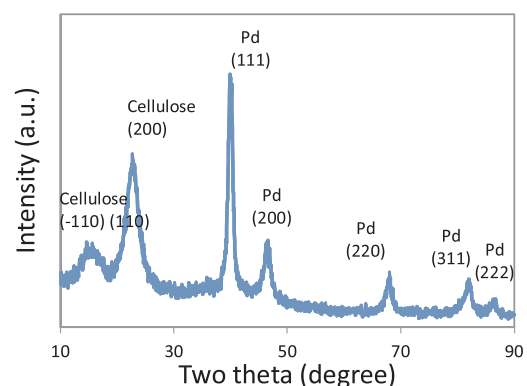


Fig. 3. XRD pattern of CNF-PdNP hybrid.

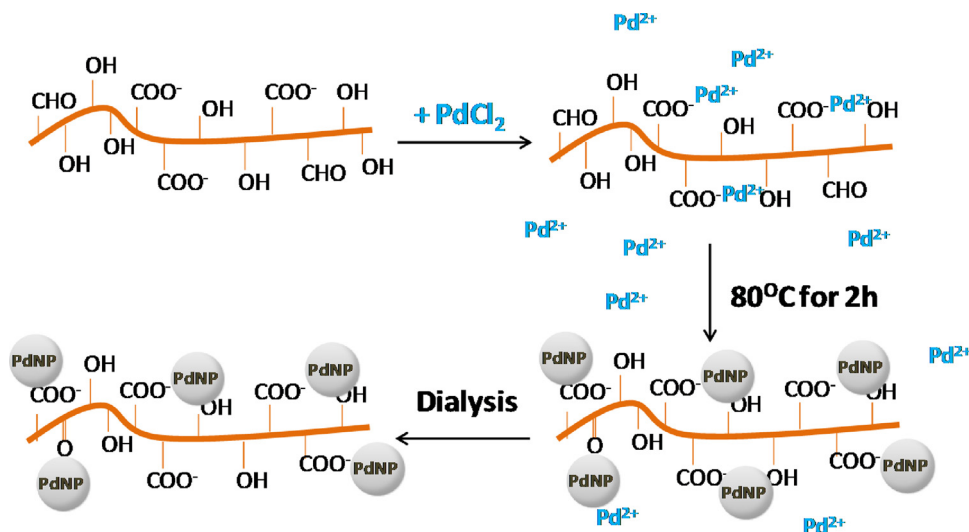


Fig. 4. Schematic illustration for the formation mechanism of PdNPs using CNFs as reducing agents and supports.

According to the Scherrer equation, the crystal sizes of Pd at (111), (200), and (311) planes were 9.0, 5.6, and 4.7 nm, respectively, corresponding to the large PdNPs observed by TEM.

Based on the above results, a possible formation mechanism of PdNPs is proposed in Fig. 4. TEMPO oxidized CNFs contained abundant carboxyls and a small amount of aldehyde groups. Under high-speed magnetic stirring, plenty of surface groups on the nano-sized CNFs were exposed to PdCl₄²⁻. The negatively charged carboxyl groups may be able to attract Pd (II) cations through electrostatic interaction. The aldehyde groups as well as some hydroxyls were responsible for the reduction of Pd (II) at relatively high temperature of 80 °C. Pd NPs were formed on the surface of the CNFs by the redox reaction. At acidic condition, CNFs aggregated as tiny gel granules [40]. The carboxyl groups and perhaps the newly formed ketone groups may be able to immobilize PdNPs by electrostatic interaction. Further dialysis process removed the unbound small NPs and the excess PdCl₂ reactants. As confirmed by TEM imaging, all the remaining PdNPs were tightly associated with the CNFs. In this study, CNF acted as the reducing agent as well as the support and no additional agent was added. Comparing to previous studies [22], our reduction condition was moderate as the hydrothermal reaction was under atmosphere pressure for just 2 h. Surface aldehyde groups formed during the TEMPO oxidation were believed to be the essential reducing agent.

3.2. Shape memory CNF aerogels decorated with Pd nanoparticles

The well dispersed aqueous suspension of CNF decorated with PdNPs was frozen at -5 °C and freeze-dried to black aerogel (Fig. 5a). The aerogel stayed intact as one cylindrical piece, shaped by the centrifuge tube, and could be easily cut into slides using a sharp razor blade without obvious deformation. The diameter of CNF-PdNP aerogel (8.2 mm) was only 55% of the inside diameter of centrifuge tube (15.0 mm). The internal structure of the aerogel was porous while the external surface was rough without any opening. The density of the CNF-PdNP aerogel was 11.6 mg/cm³. In comparison, the CNF aerogel without any Pd was white in color and fluffy (Fig. 5a), with a lower density (3.9 mg/cm³) than that of the CNF-PdNP aerogels and exhibited anisotropic porous structure as reported previously [3]. The pristine nanofibrils did not aggregate as much as their Pd-decorated counterparts during freeze-drying, as indicated by the larger diameter of the pristine CNF aerogels (11.7 mm).

The microstructure of the CNF and CNF-PdNPs aerogels was studied and compared by SEM imaging (Fig. 5b–g). The CNF aerogel contained heterogeneously shaped pores with varied sizes from several hundreds

of nanometers to more than a hundred micrometers (Fig. 5b, c). The individual nanofibrils assembled to fibers and thin films with smooth surface (Fig. 5c). The external surface of the CNF aerogel was similar to its internal structure with some open pores. In contrast, the CNF-PdNP aerogel showed less porous structure at the micro scale (Fig. 5d–g). The internal section of the aerogel exhibited a layered structure composed of smooth CNF films (Fig. 5d). At high magnification, small particles with different shapes could be seen on the cellulose surface (Fig. 5e). The particle size varied within several tens nm and was below 100 nm, revealing the presence of Pd clusters, as shown by TEM. The external surface of the aerogel was intact and mostly smooth with only few wrinkles and folds (Fig. 5f). At higher magnification (Fig. 5g), PdNP clusters were observed and the aerogel surface was rough perhaps due to the mass aggregation of nanofibrils during drying.

EDS spectra were acquired from several regions of the CNF-PdNP sample. A typical spectrum was shown in Fig. 5h. The Pd L-shell emission peak around 3 KeV is observed, while almost no Cl emission is found (< 0.4 wt%, close to the detection limit of EDS), which confirms the existence of PdNP, but not PdCl₂, on CNFs. Small amounts of sodium and platinum (< 2.0 wt %) came from the preparation process and the SEM coating, respectively. The Pd content measured by ICP-MS was 11.2 wt%.

The distinct morphology between CNF and CNF-PdNP aerogels is primarily attributed to the surface chemistry of the nanofibrils. During the slow cooling process to -5 °C, ice nucleation occurred and the well-dispersed nanofibril suspension turned into nanofibril rich domains surrounding the ice crystal. The Pd decorated CNFs were more hydrophobic and tended to exclude more water than pristine CNFs. The CNF-PdNP nanofibrils concentrated to assemble into thick films without nano-sized pores. Since the temperature first dropped at the wall of the centrifuge tube, water was slowly frozen near the wall. The CNF-PdNP nanofibrils were excluded by the ice crystal, and the resulting aggregates moved toward the center of the tube and finally formed a thick continuous film on the surface of the aerogel. However, pristine CNFs were hydrophilic and they did not self-aggregate as much as CNF-PdNPs. Thus thin fibers and porous films were observed in pristine CNF aerogels.

With interconnected structure and physical integrity, both CNF and CNF-Pd aerogels exhibited water activated shape recovery property (Supplementary movie 1 and 2). When immersed in water, CNF and CNF-PdNP aerogels were able to absorb water without noticeable change in shape. Most of the water could be easily squeezed out with tweezers and the compact aerogel could reabsorb water and return to its original size and shape within a few minutes. The fact that the

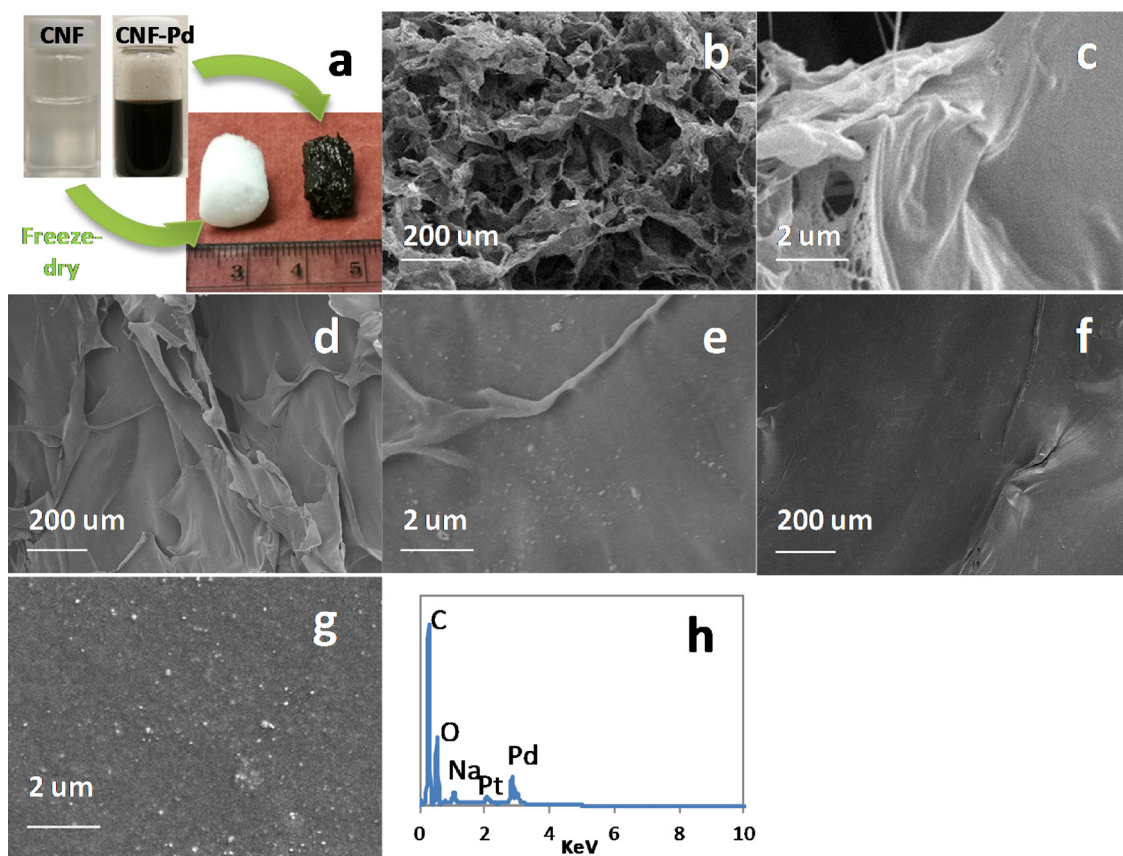


Fig. 5. Photographs and SEM images of CNF and CNF-PdNP: (a) Photographs of well dispersed CNF and CNF-PdNP suspensions and the resulting freeze-dried aerogels; (b,c) SEM images of CNF aerogel; (d, e) SEM images of internal structure of CNF-PdNP aerogel; (f,g) SEM images of external structure of CNF-PdNP aerogel; (h) Representative EDS spectrum of CNF-PdNP aerogel.

aerogel cylinders were easily squeezed to ~10% of their original diameter and quickly regained the same dimensions with a complete recovery rate, indicates that the liquid solution was able to rapidly and freely flow in and out of the material. The water-activated shape recovery property of pristine TEMPO-oxidized CNF aerogel has been reported previously [3]. It is believed that slow freezing allows the nanofibrils to concentrate and tightly associate by hydrogen bonding. The following sublimation process removes the ice templates and yields mechanically robust aerogel [3]. This is the first time that shape recovery CNF aerogels decorated with metal nanoparticles have been synthesized without any crosslinking agents. PdNPs adsorbed on the CNF surface via Coulombic attraction may disrupt the hydrogen bonding between CNFs, hence reducing the structural integrity of the aerogel. In previous studies, nanocellulose aerogels decorated with Ag nanoparticles have been synthesized in a similar way [15], but the reports did not discuss their shape memory properties and reusable potential perhaps due to the relatively weak nature of these materials. To achieve strong aerogels containing metal nanoparticles, it is critical to adequately control the surface chemistry of the pristine CNF [3], as well as the Pd content and the CNF-PdNP dispersion concentration. In addition, the aerogels derived from CNF-PdNP dispersions could be design to any shape and size based on the template container before freezing. Here, only aerogels prepared with CNF suspension concentration higher than 0.2 wt% yielded good mechanical integrity for repeating squeezing (data now shown). Potential applications of this type of aerogels include but are not limited to reusable catalysts and sensors.

3.3. Catalytic discoloration of dyes

The catalytic activity of the CNF-PdNP aerogel was evaluated based on model reactions for the catalytic reduction of organic dyes.

Methylene blue (MB) and congo red (CR) were selected as representative cationic and anionic dyes, respectively. Nobel metal nanoparticles, such as Pd, Ag and Au, can catalyze the reduction of methylene blue (MB) and Congo red (CR) in the presence of excess NaBH₄ [16,22,41]. Both MB (λ_{max} : 664 nm) and CR (λ_{max} : 498 nm) exhibit a strong absorption peak for visible light. The catalytic redox reactions were monitored at room temperature by UV-vis spectroscopy in the characteristic wavelength regions for MB and CR.

Fig. 6a illustrates the MB solution discoloration in the presence of both NaBH₄ and CNF-PdNP aerogel. Abrupt absorbance decrease was observed and the solution became completely colorless within 3 min, which is much faster than previous reports on palladium-based catalytic discoloration of MB [42,43]. It is also worth noting that these results were obtained at a much lower reducing agent to MB ratio compared to other works (i.e. NaBH₄: MB = 56:1 in this work and N₂H₄: MB = 3500:1 in [22]). Interestingly, the discoloration reaction can be speeded up further by adding more reducing agent to the solution [44]. As shown in Fig. S4, when the NaBH₄ to MB ratio increased to 529:1, more than 95% discoloration was achieved within 10 s, yielding among the highest turnover frequencies (i.e. $1.55 \text{ mol}_{\text{MB}} \cdot \text{mol}_{\text{Pd}}^{-1} \cdot \text{min}^{-1}$) reported in the literature [22,42]. In the absence of CNF-PdNP aerogel, the discoloration of the MB solution by NaBH₄ happened at an extremely slow rate, such that only a slight change in solution color was observed after three hours (Fig. S5a). The mechanism for solution discoloration can be assigned to the adsorption of MB on the nanocellulose surface and the catalytic reduction of MB in the presence of NaBH₄ and CNF-PdNP aerogel. The former involves the formation of charge-transfer complexes due to electrostatic Coulombic interactions between cationic MB and negatively charged oxygen moieties on the aerogel surface. The latter is associated with the transfer of electrons from NaBH₄ to MB, reducing the dye to a colorless form. In this case, the

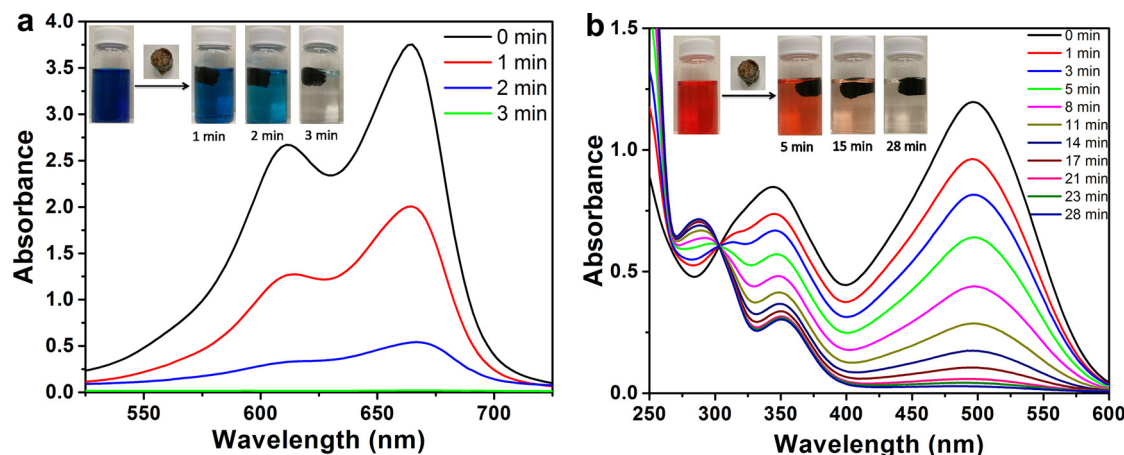


Fig. 6. Successive UV-vis spectra of the reduction of MB (a) and CR (b) catalyzed by CNF-PdNPs aerogel. Reaction conditions: $\text{NaBH}_4 = 3.5 \text{ mM}$, $\text{Pd} = 351 \mu\text{M}$, $\text{MB} = 63 \mu\text{M}$ or $\text{CR} = 29 \mu\text{M}$. The concentration of Pd was calculated based on the ICP-MS results.

reaction rate is low due to the large difference in redox potential between MB and BH_4^- and a catalyst is required. By adding CNF-PdNP aerogel to the system, the channels and pores in the aerogel allowed the MB molecules to diffuse through and contact with PdNPs, acting as an electron relay system, where the PdNPs accept electrons from BH_4^- and pass them to MB. In order to probe the contribution of MB adsorption on the solution discoloration, additional experiments were conducted in the absence of either PdNPs or NaBH_4 (Fig. S5b). Under these conditions, no MB reduction occurred and the color of the dye solution faded slowly due to uptake of MB from the solution to the surface of the aerogel. The discoloration efficiency caused by adsorption was only 16% after 3 min and barely reached 90% after more than 60 min. This reveals that the catalytic reduction of MB is the dominant effect responsible for the fast solution discoloration in the presence of NaBH_4 . The high catalytic activity of the CNF-PdNP was further demonstrated by flowing a MB and NaBH_4 aqueous mixture ($\text{MB} = 21 \mu\text{M}$, $\text{NaBH}_4 = 8.8 \text{ mM}$) through a column packed with the 3D aerogel (Supplementary movie 3). The flow rate was controlled in the $10\text{--}15 \text{ mL min}^{-1}$ range by adjusting the volume of hydrostatic head above the aerogel. The initial blue-colored solution became colorless after flowing through the CNF-PdNP aerogel and the discoloration efficiency was higher than 99%. This result exemplifies the potential of CNF-PdNP aerogels for efficient water treatment in a practical setting.

The discoloration of anionic CR solution in the presence of NaBH_4 and CNF-PdNP aerogel was also examined, as shown in Fig. 6b. A continuous decline in absorbance at 498 nm was observed as the reaction proceeded. The discoloration reached up to 97.6% after 28 min. At the same time, the absorption peak around 288 nm increased, indicating that CR had already been converted into other substance [41]. As opposed to MB discoloration, the contribution of CR adsorption on the aerogel surface was negligible due to the anionic nature of CR (Fig. S5d). The uptake of CR in the absence of NaBH_4 was below 4% after 60 min, indicating that catalytic CR reduction can be considered as the sole contribution for solution discoloration. Similarly, the reduction of CR by NaBH_4 occurred at a much slower pace in the absence of catalyst (Fig. S5c). Again, PdNPs acted as an electronic relay system, with electrons being transferred via PdNPs from BH_4^- (donor) to CR (acceptor). Furthermore, at the same mass concentration of dyes (20 mg/L), the discoloration rate of CR was much slower than MB. Besides differences in their adsorption contributions, CR ($\text{C}_{32}\text{H}_{22}\text{N}_6\text{Na}_2\text{O}_6\text{S}_2$, MW: 697 g/mol) contains two $-\text{N}=\text{N}-$ per molecule while MB ($\text{C}_{16}\text{H}_{18}\text{ClN}_3\text{S}$, MW: 320 g/mol) contains only one $-\text{N}=\text{C}-$ per molecule to accept electrons, which may influence the catalytic performance of each system.

The recovery of catalysts after use is a critical practical issue. Compared to previous work on Pd-decorated cellulose nanocrystal

(CNC) suspensions [22], the CNF aerogel catalyst can be conveniently retrieved after treatment for recycling purposes. The reusability of the CNF-PdNP aerogel was evaluated for the reduction of MB and CR (Fig. 7a, c). The reaction kinetics of each cycle was also studied and kinetics models were used to fit the data (Fig. 7b, d). For the discoloration of MB, the reaction time increased from 3 min for the first cycle to 16 min for the second cycle and reached 23–24 min for the subsequent cycles (cycles 3–5). The discoloration efficiency remained above 99.0% in each case. The longer reaction times during the last three cycles can be attributed to the saturation of adsorption sites and the possible decrease in catalytic activity. Since the uptake capacity of the aerogel is unlikely recovered by simple squeezing between cycles, the number of adsorption sites occupied by MB increases gradually over time until all sites are saturated and MB can no longer be adsorbed, such that only the reduction reaction could decolorize the solution after a certain time. Interestingly, the reaction rate of each individual cycle remained almost constant over time, indicating that the reaction rate was independent on the concentration of the reactants during the reaction. The linear correlation between $(A_0 - A_t)$ versus time for each cycle (Fig. 7b, $R^2 > 0.92$) confirms that the MB reduction follows a pseudo-zero-order reaction kinetics. Pseudo-zero-order reaction commonly occurs when the reaction is catalyzed by attachment to a solid surface (heterogeneous catalysis). In our system, PdNPs were associated with the solid CNF network and the reaction generally occurred at the solid-liquid interface. The kinetic constants are calculated from the slopes of the fitting curves and determined to be $1.384 \text{ min}^{-1} \text{ A}$, $0.246 \text{ min}^{-1} \text{ A}$, $0.178 \text{ min}^{-1} \text{ A}$, $0.178 \text{ min}^{-1} \text{ A}$, $0.172 \text{ min}^{-1} \text{ A}$ for the five successive cycles, respectively. Again, these values are higher than previously reported rate constants under similar conditions [42,43].

Fig. 7c shows the reusability of the CNF-PdNP aerogel for the discoloration of CR solutions. The reaction time increased from 28 min for the first cycle to 45–50 min for the second and subsequent cycles. The discoloration efficiency was still higher than 91% after the fifth cycle. As opposed to MB discoloration, the reaction rate of each individual cycle decreased with reaction time. The linear correlation between $\ln(A_0/A_t)$ versus time in minutes for each cycle (Fig. 7d, $R^2 > 0.98$) indicates that the CR reduction follows a pseudo-first-order reaction kinetics. The kinetic constants are calculated from the slopes of the fitting curves and determined to be 0.140 min^{-1} , 0.067 min^{-1} , 0.072 min^{-1} , 0.068 min^{-1} , 0.053 min^{-1} for five successive cycles, respectively. In previous studies, pseudo-first-order reaction kinetics has been reported for the catalytic reduction of organic dyes with nanocellulose film [45] or other nature polysaccharides [46] supported noble metals in the presence of an excess amount of NaBH_4 . This means that the reaction rate is dependent on the concentration of the dyes. Our results of CR are consistent with those studies. Both the reduction rate and reduction

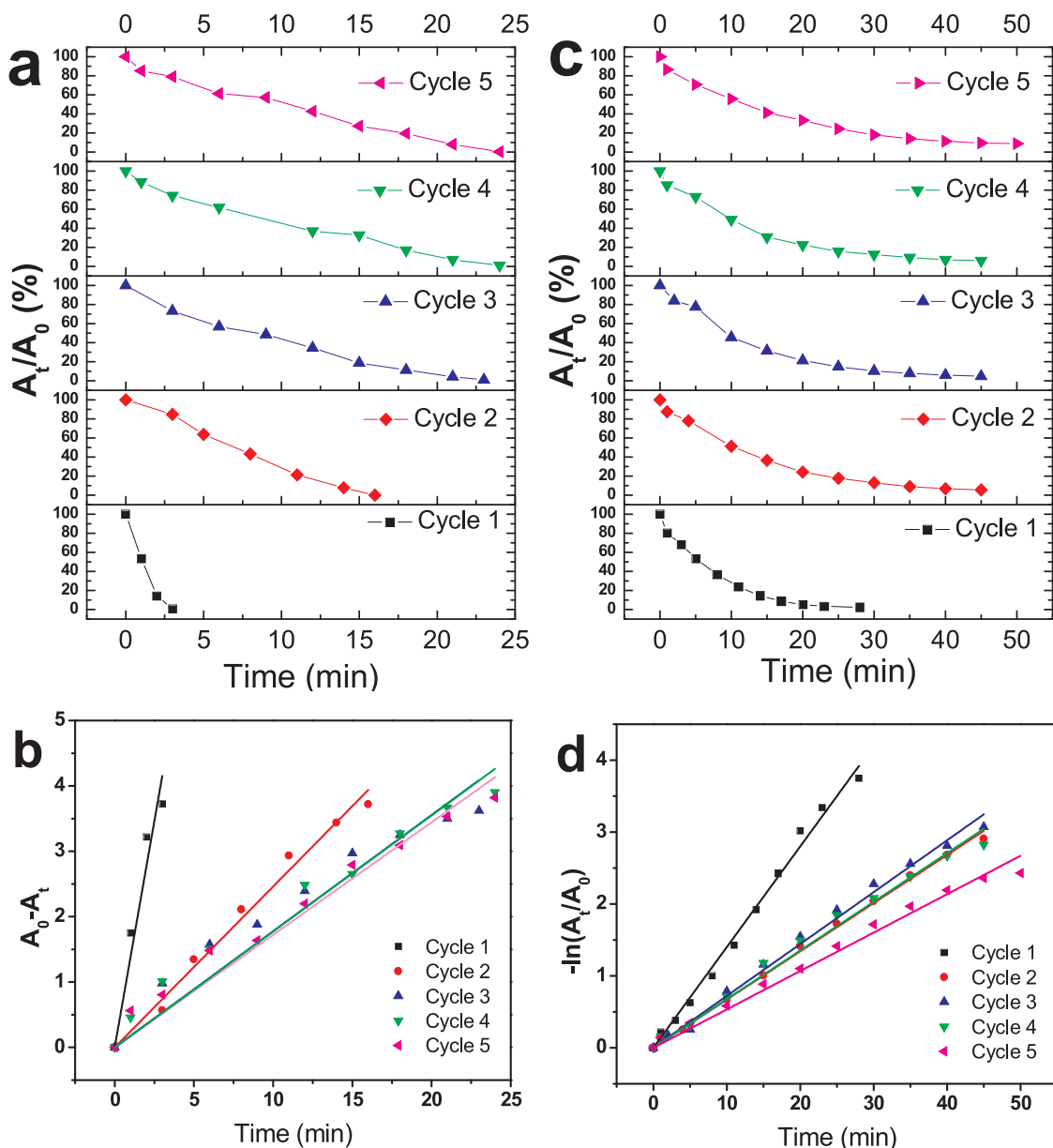


Fig. 7. Reusable reductions of dyes for five successive cycles with the same batch of CNF-PdNPs aerogel: (a) Reusable reductions of MB as a function of time for five successive cycles; (b) plot of $(A_t - A_0)$ against time used in each MB reduction cycle; (c) Reusable reductions of CR as a function of time for five successive cycles; (d) plot of $-\ln(A_t/A_0)$ against time used in each CR reduction cycle. All reaction conditions were the same as in Fig. 6.

efficiency of CR were lower than for MB. The variations in reaction kinetics between MB and CR may be due the different adsorption and catalytic behaviors of the aerogels to each dye. Furthermore, a slow deactivation of the catalyst was observed over time as indicated by the gradual reduction of the kinetic constants with successive cycling tests. The relatively slow uptake of dyes on CNF binding sites cannot solely explain the decrease in kinetic constants. Moreover, limited palladium leaching was expected, considering the CNF-PdNP aerogels were systematically dialyzed against water for extending periods of time prior to dye discoloration. A recent study using mesoporous basswood decorated with Pd nanoparticles for catalytic dye discoloration confirmed that no Pd leached into the aqueous effluent during treatment [47]. Possible catalyst poisoning may occur due the presence of sodium from the reducing agent. The adsorption of sodium has been reported to cause serious palladium poisoning in different catalytic systems [48]. Therefore, the possible migration of sodium adsorbed on the CNF surface to the Pd nanoparticles may induce the slow catalytic deactivation

observed in Fig. 7. In addition, the aggregation of PdNPs with reaction time might also contribute to the reduction of the catalyst activity. Overall, the CNF-PdNP aerogels exhibit excellent recyclability for catalytic reduction of both MB and CR for several cycles.

4. Conclusion

CNF-PdNPs were obtained by the simple reduction of PdCl_2 using CNF as both stabilizer and reducing agent at 80 °C for 2 h. Water activated shape memory CNF-PdNPs aerogels were prepared by freeze-drying the nanohybrid dispersion. The nanohybrid materials were characterized by TEM, HRTEM, EDS, XRD, SEM, AFM, UV-vis absorption spectroscopy and conductometric titration. Aldehyde content on CNFs functions as effective agents to reduce $\text{Pd}(\text{II})$ ions to PdNPs. The PdNPs immobilized on CNFs with a diameter range of 1–20 nm and formed cluster structure consisting of many tiny particles. The catalytic properties of the aerogels were examined in the framework of dye

discoloration in aqueous solution. The results indicate that both cationic (MB) and anionic (CR) solutions with an initial concentration of 20 mg/L can be reduced to colorless forms in less than 3 and 30 min, respectively. The catalysts exhibited high turnover frequencies and can be successfully applied to packed column systems for continuous flow water purification. In addition, the CNF-PdNP aerogels show excellent reusability and maintained 91.1–99.0% discoloration efficiency for at least five successive cycles. Hence, the developed reagentless green process significantly widens the scope of CNF aerogels decorated with metal nanoparticles, particularly in catalysis and environmental remediation.

Acknowledgements

The authors are grateful that this research was financially supported by the Guangdong Provincial Department of Science and Technology (Project #2017B020238003), the USDA National Institute of Food and Agriculture (McIntire Stennis project #1009515), and the Bureau of Guangdong Forestry (Project #4900-F16304). We also acknowledge Dr. Kunlin Song and Heather Wise at UW for their assistance with TEM and SEM observations, respectively.

Appendix A. Supplementary data

Supplementary material related to this article can be found, in the online version, at doi:<https://doi.org/10.1016/j.apcatb.2018.06.002>.

References

- [1] K.J. De France, T. Hoare, E.D. Cranston, Review of hydrogels and aerogels containing nanocellulose, *Chem. Mater.* 29 (11) (2017) 4609–4631.
- [2] F. Jiang, Y.-L. Hsieh, Amphiphilic superabsorbent cellulose nanofibril aerogels, *J. Mater. Chem. A* 2 (2014) 6337–6342.
- [3] F. Jiang, Y.-L. Hsieh, Super water absorbing and shape memory nanocellulose aerogels from TEMPO-oxidized cellulose nanofibrils via cyclic freezing–thawing, *J. Mater. Chem. A* 2 (2014) 350–359.
- [4] S. Zhou, P. Liu, M. Wang, H. Zhao, J. Yang, F. Xu, Sustainable, reusable, and superhydrophobic aerogels from microfibrillated cellulose for highly effective oil/water separation, *ACS Sustain. Chem. Eng.* 4 (2016) 6409–6416.
- [5] X. Yang, E.D. Cranston, Chemically cross-linked cellulose nanocrystal aerogels with shape recovery and superabsorbent properties, *Chem. Mater.* 26 (2014) 6016–6025.
- [6] J.T. Korhonen, P. Hiekkataipale, J. Malm, M. Karppinen, O. Ikkala, R.H. Ras, Inorganic hollow nanotube aerogels by atomic layer deposition onto native nanocellulose templates, *ACS Nano* 5 (2011) 1967–1974.
- [7] G. Ye, X. Zhu, S. Chen, D. Li, Y. Yin, Y. Lu, S. Komarneni, D. Yang, Nanoscale engineering of nitrogen-doped carbon nanofiber aerogels for enhanced lithium ion storage, *J. Mater. Chem. A* 5 (2017) 8247–8254.
- [8] B. Seantier, D. Bendahou, A. Bendahou, Y. Grohens, H. Kaddami, Multi-scale cellulose based new bio-aerogel composites with thermal super-insulating and tunable mechanical properties, *Carbohydr. Polym.* 138 (2016) 335–348.
- [9] M.S. Toivonen, A. Kaskela, O.J. Rojas, E.I. Kauppinen, O. Ikkala, Ambient-dried cellulose nanofibril aerogel membranes with high tensile strength and their use for aerosol collection and templates for transparent, flexible devices, *Adv. Funct. Mater.* 25 (2015) 6618–6626.
- [10] D.O. Carlsson, G. Nyström, Q. Zhou, L.A. Berglund, L. Nyholm, M. Strömme, Electroactive nanofibrillated cellulose aerogel composites with tunable structural and electrochemical properties, *J. Mater. Chem.* 22 (2012) 19014–19024.
- [11] C. Gebald, J.A. Wurzbacher, P. Tingaut, T. Zimmermann, A. Steinfeld, Amine-based nanofibrillated cellulose as adsorbent for CO₂ capture from air, *Environ. Sci. Technol.* 45 (2011) 9101–9108.
- [12] J.C. Arboleda, M. Hughes, L.A. Lucia, J. Laine, K. Ekman, O.J. Rojas, Soy protein–nanocellulose composite aerogels, *Cellulose* 20 (2013) 2417–2426.
- [13] X. Zhang, Y. Wang, J. Zhao, M. Xiao, W. Zhang, C. Lu, Mechanically strong and thermally responsive cellulose nanofibers/poly(N-isopropylacrylamide) composite aerogels, *ACS Sustain. Chem. Eng.* 4 (2016) 4321–4327.
- [14] K. Gao, Z. Shao, X. Wang, Y. Zhang, W. Wang, F. Wang, Cellulose nanofibers/multi-walled carbon nanotube nanohybrid aerogel for all-solid-state flexible supercapacitors, *RSC Adv.* 3 (2013) 15058–15064.
- [15] S.W. Chook, C.H. Chia, C.H. Chan, S.X. Chin, S. Zakaria, M.S. Sajab, N.M. Huang, A porous aerogel nanocomposite of silver nanoparticles-functionalized cellulose nanofibrils for SERS detection and catalytic degradation of rhodamine b, *RSC Adv.* 5 (2015) 88915–88920.
- [16] M. Kaushik, A. Moores, Nanocelluloses as versatile supports for metal nanoparticles and their applications in catalysis, *Green Chem.* 18 (2016) 622–637.
- [17] J. Feng, C. Yang, D. Zhang, J. Wang, H. Fu, H. Chen, X. Li, Catalytic transfer hydrogenolysis of α-methylbenzyl alcohol using palladium catalysts and formic acid, *Appl. Catal. A* 354 (2009) 38–43.
- [18] C.M. Cirtiu, A.F. Dunlop-Briere, A. Moores, Cellulose nanocrystallites as an efficient support for nanoparticles of palladium: application for catalytic hydrogenation and heck coupling under mild conditions, *Green Chem.* 13 (2011) 288–291.
- [19] L.S. Søbjerg, D. Gauthier, A.T. Lindhardt, M. Bunge, K. Finster, R.L. Meyer, T. Skrydstrup, Bio-supported palladium nanoparticles as a catalyst for Suzuki–Miura and Mizoroki–Heck reactions, *Green Chem.* 11 (2009) 2041–2046.
- [20] P. Zhou, H. Wang, J. Yang, J. Tang, D. Sun, W. Tang, Bacteria cellulose nanofibers supported palladium(0) nanocomposite and its catalysis evaluation in heck reaction, *Ind. Eng. Chem. Res.* 51 (2012) 5743–5748.
- [21] M. Rezayat, R.K. Blundell, J.E. Camp, D.A. Walsh, W. Thielemans, Green one-step synthesis of catalytically active palladium nanoparticles supported on cellulose nanocrystals, *ACS Sustain. Chem. Eng.* 2 (2014) 1241–1250.
- [22] X. Wu, C. Lu, W. Zhang, G. Yuan, R. Xiong, X. Zhang, A novel reagentless approach for synthesizing cellulose nanocrystal-supported palladium nanoparticles with enhanced catalytic performance, *J. Mater. Chem. A* 1 (2013) 8645–8652.
- [23] A. Safavi, N. Maleki, M.M. Doroodmand, Fabrication of a room temperature hydrogen sensor based on thin film of single-walled carbon nanotubes doped with palladium nanoparticles, *J. Exp. Nanosci.* 8 (2013) 717–730.
- [24] S. Thiagarajan, R.-F. Yang, S.-M. Chen, Palladium nanoparticles modified electrode for the selective detection of catecholamine neurotransmitters in presence of ascorbic acid, *Bioelectrochemistry* 75 (2009) 163–169.
- [25] G. Yang, J. Xie, Y. Deng, Y. Bian, F. Hong, Hydrothermal synthesis of bacterial cellulose/AgNPs composite: a “green” route for antibacterial application, *Carbohydr. Polym.* 87 (2012) 2482–2487.
- [26] H. Duan, D. Wang, Y. Li, Green chemistry for nanoparticle synthesis, *Chem. Soc. Rev.* 44 (2015) 5778–5792.
- [27] Á. Molnár, A. Papp, The use of polysaccharides and derivatives in palladium-catalyzed coupling reactions, *Catal. Sci. Technol.* 4 (2014) 295–310.
- [28] H.-Y. Yu, Z.-Y. Qin, B. Sun, C.F. Yan, J.-M. Yao, One-pot green fabrication and antibacterial activity of thermally stable corn-like CNC/Ag nanocomposites, *J. Nanopart. Res.* 16 (2014) 1–12.
- [29] H. Dong, J.F. Snyder, D.T. Tran, J.L. Leadore, Hydrogel, aerogel and film of cellulose nanofibrils functionalized with silver nanoparticles, *Carbohydr. Polym.* 95 (2013) 760–767.
- [30] R. Xiong, C. Lu, W. Zhang, Z. Zhou, X. Zhang, Facile synthesis of tunable silver nanostructures for antibacterial application using cellulose nanocrystals, *Carbohydr. Polym.* 95 (2013) 214–219.
- [31] L. Johnson, W. Thielemans, D.A. Walsh, Nanocomposite oxygen reduction electrocatalysts formed using biodegradable reducing agents, *J. Mater. Chem.* 20 (2010) 1737–1743.
- [32] X. Wu, C. Lu, Z. Zhou, G. Yuan, R. Xiong, X. Zhang, Green synthesis and formation mechanism of cellulose nanocrystal-supported gold nanoparticles with enhanced catalytic performance, *Environ. Sci.: Nano* 1 (2014) 71–79.
- [33] Y. Shin, J.M. Blackwood, I.-T. Bae, B.W. Arey, G.J. Exarhos, Synthesis and stabilization of selenium nanoparticles on cellulose nanocrystal, *Mater. Lett.* 61 (2007) 4297–4300.
- [34] Y. Shin, I.-T. Bae, B.W. Arey, G.J. Exarhos, Simple preparation and stabilization of nickel nanocrystals on cellulose nanocrystal, *Mater. Lett.* 61 (2007) 3215–3217.
- [35] J. Gu, Y.-L. Hsieh, Surface and structure characteristics, self-assembling, and solvent compatibility of holocellulose nanofibrils, *ACS Appl. Mater. Interfaces* 7 (2015) 4192–4201.
- [36] T. Saito, A. Isogai, TEMPO-mediated oxidation of native cellulose. The effect of oxidation conditions on chemical and crystal structures of the water-insoluble fractions, *Biomacromolecules* 5 (2004) 1983–1989.
- [37] A. Isogai, T. Saito, H. Fukuzumi, TEMPO-oxidized cellulose nanofibers, *Nanoscale* 3 (2011) 71–85.
- [38] S. Kundu, S.-I. Yi, L. Ma, Y. Chen, W. Dai, A.M. Sinyukov, H. Liang, Morphology dependent catalysis and surface enhanced Raman scattering (SERS) studies using Pd nanostructures in DNA, CTAB and PVA scaffolds, *Dalton Trans.* 46 (2017) 9678–9691.
- [39] V.L. Nguyen, D.C. Nguyen, H. Hirata, M. Ohtaki, T. Hayakawa, M. Nogami, Chemical synthesis and characterization of palladium nanoparticles, *Adv. Nat. Sci.: Nanosci. Nanotechnol.* 1 (2010) 035012.
- [40] Y. Okita, S. Fujisawa, T. Saito, A. Isogai, TEMPO-oxidized cellulose nanofibrils dispersed in organic solvents, *Biomacromolecules* 12 (2011) 518–522.
- [41] X. Liu, M. Liang, M. Liu, R. Su, M. Wang, W. Qi, Z. He, Highly efficient catalysis of azo dyes using recyclable silver nanoparticles immobilized on tannic acid-grafted eggshell membrane, *Nanosc. Res. Lett.* 11 (2016) 440.
- [42] G. Fu, L. Tao, M. Zhang, Y. Chen, Y. Tang, J. Lin, T. Lu, One-pot, water-based and high-yield synthesis of tetrahedral palladium nanocrystal decorated graphene, *Nanoscale* 5 (2013) 8007–8014.
- [43] G. Fu, X. Jiang, L. Ding, L. Tao, Y. Chen, Y. Tang, Y. Zhou, S. Wei, J. Lin, T. Lu, Green synthesis and catalytic properties of polyallylamine functionalized tetrahedral palladium nanocrystals, *Appl. Catal. B: Environ.* 138 (2013) 167–174.
- [44] S. Li, H. Li, J. Liu, H. Zhang, Y. Yang, Z. Yang, L. Wang, B. Wang, Highly efficient degradation of organic dyes by palladium nanoparticles decorated on 2D magnetic reduced graphene oxide nanosheets, *Dalton Trans.* 44 (2015) 9193–9199.
- [45] B. Ramaraju, T. Imae, A.G. Destage, Ag nanoparticle-immobilized cellulose nanofibril films for environmental conservation, *Appl. Catal. A* 492 (2015) 184–189.
- [46] B.R. Ganaparam, M. Alle, R. Dadigala, A. Dasari, V. Maragoni, V. Guttena, Catalytic reduction of methylene blue and Congo red dyes using green synthesized gold nanoparticles capped by salmalia malabarica gum, *Int. Nano Lett.* 5 (2015) 215–222.
- [47] F. Chen, A.S. Gong, M. Zhu, G. Chen, S.D. Lacey, F. Jiang, Y. Li, et al., 683 mesoporous, three-dimensional wood membrane decorated with nanoparticles for 684 highly efficient water treatment, *ACS Nano* 11 (2017) 4275–4282 22 685.
- [48] I.V. Yentekatis, R.M. Lambert, M. Konsolakis, V. Kiousis, The effect of sodium on 686 the Pd-catalyzed reduction of NO by methane, *Appl. Catal. B: Environ.* 18 (687) (1998) 293–305.